Journal of Materials Chemistry B

Accepted Manuscript

ROYAL SOCIETY OF CHEMISTRY

www.rsc.org/materialsB

Cite this: DOI: 10.1039/c0xx00000x

www.rsc.org/xxxxxx

Paper

Self-assembly-induced near-infrared fluorescence nanoprobes for effective tumor molecular imaging

Hao Wu[a,b], Haidong Zhao[c], Xiaojie Song[a,b], Shen Li[a,b], Xiaojun Ma[a,*], and Mingqian Tan[a,*]

Received (in XXX, XXX) Xth XXXXXXXXX 20XX, Accepted Xth XXXXXXXXX 20XX
DOI: 10.1039/b000000x

Fabrication of near-infrared (NIR) fluorescence nanoprobes (NPs) has drawn great attention due to their potential as highly sensitive optical probes for *in vivo* tumor molecular imaging. Herein, a facile strategy was reported for the preparation of ultrasmall (<20 nm) indocyanine green (ICG)-containing NIR fluorescence NPs using self-assembly chemistry between folate (FA) modified water-soluble chitosan (WCS) and ICG. The ICG-containing NPs exhibit characteristics of crystalline solid, good photostability, lower cytotoxicity and high tumor targeting ability for in vitro cell imaging. We also explored this system for in vivo tumor molecular imaging. Significant tumor accumulation was observed for both in vitro and in vivo tumor imaging in HeLa tumor cell imaging and xenograft-bearing mice model (2 μmol·kg^{-1} at 48 and 72 h time points). The availability of these self-assembled NIR NPs provides a convenient tool for tumor imaging and detection.

1. Introduction

Near-infrared (NIR) tumor molecular imaging is emerging as a promising real-time, high-resolution and noninvasive modality to provide molecular information of the tumor tissue for cancer detection, assessment of tumor treatment and drug discovery, which greatly relies on the synthesis of tumor-selective and sensitive probes.[1-4] Multifunctional nanoprobes (NPs) for simultaneous tumor targeting and NIR fluorescence imaging are highly desired because of their good tumor selectivity, negligible background autofluorescence and high tissue penetration at the NIR window of 650-900 nm.[5-7] A variety of organic dyes are expected to have potential for clinical implications as non-targeting tumor optical imaging agents in which indocyanine green (ICG) proved by the Federal Drug Administration (FDA) for clinical human medical imaging and diagnosis.[8] Owing to its capacity to absorb and emit in the NIR spectral range and low toxicity, ICG has been widely applied in disease diagnosis including the test of cardiac output, hepatic function and ophthalmic perfusion.[9-12] However, as a small molecular agent, ICG suffers from the drawbacks of concentration-depended aggregation, poor photostability, fast clearance rate from the body with a short half-life about 2-4 min, non-specific binding to most of the plasma proteins and lack of tumor selectivity.[13] In addition, ICG is mainly eliminated from the liver and secreted entirely into the bile and does not undergo renal excretion.[8, 14] All these drawbacks restrict its utility in effective and prolonged tumor molecular imaging. Recently, to overcome these limitations, ICG-containing nanocarriers such as micellar encapsulation system,[15, 16] poly (lactic-co-glycolic acid) (PLGA) nanoparticles (> 300 nm),[17, 18] folate(FA)-amphiphilic chitosan micelles (~136 nm),[19] inorganic silica/calcium phosphate nanoparticles,[20, 21] have been reported for ICG delivery in tumor imaging. While these nanocarriers are generally very useful for improving the ICG molecule stability or prolong its plasma half-life, the complicated nanostructure still suffer from poor hydrophilicity, lacking active targeting effect, existence of excess surfactants, tedious synthesis process, the use of toxic organic solvent or relatively large size. Therefore, there is a great need to overcome these drawbacks. Alternatively, ICG-containing NPs have been successfully constructed by using simple self-assembly chemistry between phospholipid-polyethylene glycol (PL-PEG) and ICG for *in vitro* tumor cell imaging.[22] This has motivated us to search for an efficient strategy for the controllable synthesis of ICG-containing NPs for effective *in vivo* tumor-targeted optical imaging.

In this paper, we reported a facile method to prepare crystalline ultrasmall (<20 nm) ICG-containing NIR fluorescence NPs using self-assembly chemistry between FA modified water-soluble chitosan (WCS) and ICG for *in vivo* tumor-targeted optical imaging. To the best of our knowledge, this is the first report about preparation of the NIR fluorescence NPs which can achieve active accumulation in tumor by such a simple self-assembling strategy. Chitosan has been widely used in pharmaceutics, regeneration medicine and tissue engineering owing to its nontoxic, biodegradable, biocompatible, and antimicrobial properties.[23-25] FA is a major vitamin that is essential nutrient substance for cell proliferation and maintenance of rapid cell division and growth.[26] FA receptors (FRs)[27] are over-expressed on the cell membranes of many carcinoma cells,[28] including cervical cancer, thus we choose folic acid to target the NPs. The self-assembled NPs of FA-modified water-soluble chitosan are attractive for ICG delivery in tumor molecular imaging because of the following reasons. (1) The NPs, being composed of WCS and FA, are biocompatible, biodegradable and nontoxic. (2) By selecting WCS as ICG carrier, this strategy overcomes the drawback that chitosan is easily aggregation in aqueous solution at physiological pH. (3) The FA modified NPs

having size of approximate 10 nm in diameter can achieve both passive and active targeting effect, which will increase the tumor accumulation in molecular imaging. (4) As carrier materials, FA modified WCS is able to stabilize the ICG molecules avoiding the bleaching and excited light damage during the process of *in vivo* tumor imaging. (5) The synthesis of ICG-containing NIR fluorescence NPs is simple, rapid, effective and labor-saving, which only takes about 20 seconds and can be performed at neutral pH in aqueous solution. Thus, this strategy can be developed as a general method for the delivery of drugs, genes, and other biomolecules, where the fluorescence signal of ICG would then monitor the release, biodistribution of these cargos or assess the therapeutic effect as well.

2. Experimental section

2.1 Materials

Indocyanine green was purchased from Yichuang Company Ltd. (Dandong, China). Chitosan (19.8 KDa, degree of deacetylation (DD) = 95%) was purchased from Yuhuan Company Ltd. (Zhejiang, China). FA was purchased from CapitailBio Corporation (Shanghai, China). (1-ethyl-3-(3-dimethyl aminopropyl) carbodiimide, hydrochloride, EDC·HCl) was purchased from Acros Organics (USA). Chinese hamster ovary (CHO) cell line was a gift kindly provided by Institute of Biochemistry and Cell Biology, Shanghai Institute for Biological Sciences, Chinese Academy of Sciences. Cervical carcinoma cell Hela cell line, breast carcinoma cell MCF-7 cell line and liver carcinoma cell 7721 cell line were purchased from Nanjing KeyGen Biotech. Co. Ltd. (Nanjing, China).

2.2 Instruments

High-resolution transmission electron microscopy (HRTEM) images were collected on an electron microscope (JEM-2100, JEOL), using a 200 kV accelerating voltage. The fourier transform infrared (FTIR) spectra were measured by VECTOR 22 with the KBr pellet technique ranging from 500 to 4000 cm^{-1}. Zeta potential measurements were performed on a Zetasizer Nanoseries (ZS, Malvern). Absorption and fluorescent spectra were recorded by UV-Vis spectrophotometer (UV-2550, SHIMADZU) and fluorospectro photometer (LS-55, Perkin Elmer), respectively. Statistical analysis was performed using a two-way ANOVA with Bonferroni's, assuming statistical significance at $p < 0.05$. *In vivo* imaging was carried out with a CRi Meastro Ex *in vivo* imaging system (Caliper Life Sciences Inc. USA.).

2.3 Synthesis of FA-WCS

WCS with molecular weight of 19.8 kDa was degraded and acetylated from the raw material (Yuhuan Ocean Biomaterials Corporation, Zhejiang, China). The DD was 50% as determined by FTIR. In a round-bottom flask, 6 mg of FA and 13.2 mg of EDC were dissolved in 5 mL of phosphate buffered saline (PBS) and the mixture was activated in dark for 30 min. Subsequently, the mixture was added dropwise to 15 mL of WCS (20 mg/mL) PBS solution. After 16 h of continuous stirring at room temperature, the FA-WCS aqueous solution was obtained by dialysis against pure water to remove the impurities. The FA-WCS aqueous solution was lyophilized to obtain the pure FA-WCS. The FA grafting degree of the FA-WCS was 0.74% determined by spectrophotometric method at 363 nm. ^{1}H NMR (400 MHz, D_2O, δ) for WCS: 2.043 (s, -$COCH_3$), 2.751(m, H2 of glucosamine), 3.547-3.920 (m, H3, H4, H5, H6 of glucosamine), 4.527(m, H1 of glucosamine); ^{1}H NMR (400 MHz, D_2O, δ) for FA-WCS: 2.049(s, -$COCH_3$), 2.867(m, H2 of FA-glucosamine), 3.132-3.195 (m, H-folic acid), 3.549-3.923 (m, H3, H4, H5, H6 of FA-glucosamine), 3.761(m, H-folic acid), 4.608(m, H1 of FA-glucosamine), 6.790 (m, H-Aromatic ring of folic acid) (Fig. S1).

2.4 Synthesis of ICG-FA-WCS and ICG-WCS NPs

ICG-FA-WCS or ICG-WCS NPs were synthesized via self-assembling method by adding 0.2 mL of FA-WCS or WCS solution at different concentrations (0.25%, 0.125%, 0.1%, 0.0833% or 0.0625%, wt/wt) to 1mL of ICG aqueous solution with vortex for 20 s.

2.5 Cell Viability Study

CHO cells (Chinese hamster ovary) were seeded in 96-well plates at a density of 5×10^3 cells/well and cultured for 24 h in 10% serum containing DMEM medium supplemented with penicillin (100 units·mL^{-1}) and streptomycin (100 μg·mL^{-1}) in a humidified atmosphere with 5% CO_2 at 37°C. After incubation with different concentrations (0, 0.004, 0.008, 0.016, 0.032, 0.063, 0.125, 0.250, 0.500 mg·mL^{-1}, n=3) of ICG-FA-WCS NPs for 24 h, 20 μL of MTT (5 mg·mL^{-1}) reagent was added to each cell well. After further incubation for 4 h, the cells were washed with PBS three times and 100μL of dimethylsulfoxide (DMSO) was added. The optical density (OD) of the mixture was measured at 570 nm using a Microplate Reader (Wellscan MK3, Labsystems). The cell viability was estimated according to the following equation: Cell Viability [%] = ($OD_{treated}$ /$OD_{control}$) × 100% ($OD_{control}$ is measured in the absence of agent, and $OD_{treated}$ donates the intensity obtained in the presence of ICG NPs.

2.6 Animal tumor model

All animal care and experimental procedures were approved by the Animal Care Committees of the Dalian Medical University. Female BALB/c-nu mice (5-6 weeks) were purchased from the Animal Center of Dalian Medical University. The mice were subcutaneously implanted in flank with 1×10^6 Hela cells in a mixture of 50 μL of culture medium and 50 μL of Matrigel. The optical imaging study was performed when the tumor size reached 0.3-0.5 cm in diameter in 2-3 weeks.

2.7 *In vitro* cellular Imaging

Hela (human cervical cancer), MCF-7 (human breast cancer) and 7721 (human liver cancer) cells were seeded in 24-well plates at a density of 5×10^3 cells/well, respectively. After incubation with the agents (free ICG, ICG-WCS, ICG-FA-WCS NPs, 31μg·mL^{-1}, calculated for ICG) in fresh medium for 4 h, the cells were washed by PBS three times and imaged with Maestro EX *in vivo* imaging system and the relative fluorescence intensity was calculated with Maestro software (Cambridge Research & Instrumentation, Inc, Woburn, MA).

2.8 *In vivo* tumor imaging

The mice were anesthetized by 2 % isoflurane and imaged on a Maestro EX *in vivo* imaging system after injection of NPs or free

ICG from the tail vein at a dose of 2 μmol·kg^{-1} body weight. Spectral fluorescence images were obtained using the appropriate filter for ICG (excitation: 735 nm; maximum emission: 805 nm; acquisition settings: 780-900 in 10 nm steps, long-pass filter). Exposure times were automatically calculated for free ICG, ICG-WCS and ICG-FA-WCS NPs. To obtain quantitative results, the ICG signal was spectrally extracted from the multispectral fluorescence images with Maestro software after subtracting the background auto-fluorescence and regions of interest (ROIs) were selected over the tumors. Average signal values in tumor ROIs (N=6) were normalized to the non-tumor ROI. Statistical analysis was performed using Origin 8 software (Origin Lab Corp.). To assess binding, the mice were sacrificed and the tumors and various organs were imaged on the Maestro EX *in vivo* imaging system according to the above protocol at 48 h after administration. As for histochemical analyses, tumor tissues were cryosectioned into 6-μm slices and imaged immediately at 20 X on aTCS-SP2 Leica confocal laser scanning microscope.

3. Results and discussion

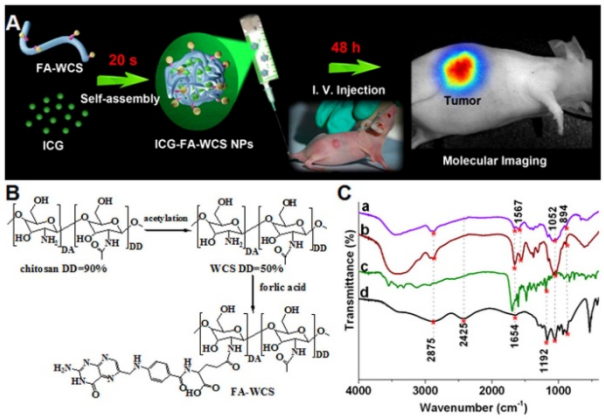

Fig.1 (A) Schematic illustration of ICG-containing NPs through self-assembly of FA-modified WCS and ICG for *in vivo* tumor molecular imaging. (B) Synthesis scheme for the preparation of FA-WCS. (C) FTIR spectra of DD 90% chitosan (a), WCS (DD, 50%) (b), FA (c) and FA-WCS (d), respectively.

Fig.1A summarizes the self-assembled NIR fluorescence NPs for *in vivo* tumor-targeted optical imaging. Synthesis of the NIR fluorescence NPs includes three steps: (1) acid-free WCS with DD 50% was prepared by reacting of DD 90% chitosan with acetic anhydride (Fig. 1B);[29] (2) FA-WCS was synthesized by incorporating FA to DD 50% WCS via one-step amidation reaction; (3) ICG-containing NPs were prepared by vortex of WCS or FA-WCS with ICG for 20 seconds at neutral pH in aqueous solution. The prepared NPs were then characterized by FTIR spectra. As shown in Fig. 1C, FTIR results have clearly demonstrated the formation of DD 50% WCS and the conjugate of FA-WCS. First, the peak at 1654 cm^{-1} of FTIR spectra assigned to amide streching vibration of WCS in Fig. 1C (b) increases as compared with that of DD 90% chitosan (Fig. 1C (a)) and the peak at 1567 cm^{-1} caused by -NH_2 aborption of WCS (Fig. 1C (b)) decreases than that of DD 90% chitosan (Fig. 1C (a)), indicating WCS has smaller DD than DD 90% chitosan. The calculated DD was about 50% as determined by comparing the ratio of the peak at 1567 cm^{-1} and 1654 cm^{-1}. Second, as shown in Fig. 1C(d), the spectrum of FA-WCS conjugate displays not only the characteristic peaks of WCS at 2875, 1654, 1052, and 894 cm^{-1} but also the characteristic band of FA at 1192 cm^{-1} (Fig.1C (c)). This result clearly indicates that the FA has been successfully conjugated onto WCS. The calculated FA grafting percent of FA-WCS is about 0.74%. The presence of targeting moiety FA on the conjugate of FA-WCS was further confirmed by ^{1}H-NMR spectra shown in Fig. S1A, which clearly shows the signal assigned to the H of folic acid as compared with that of WCS. All these results demonstrated that the FA modified WCS was successfully synthesized through one-step amidation reaction.

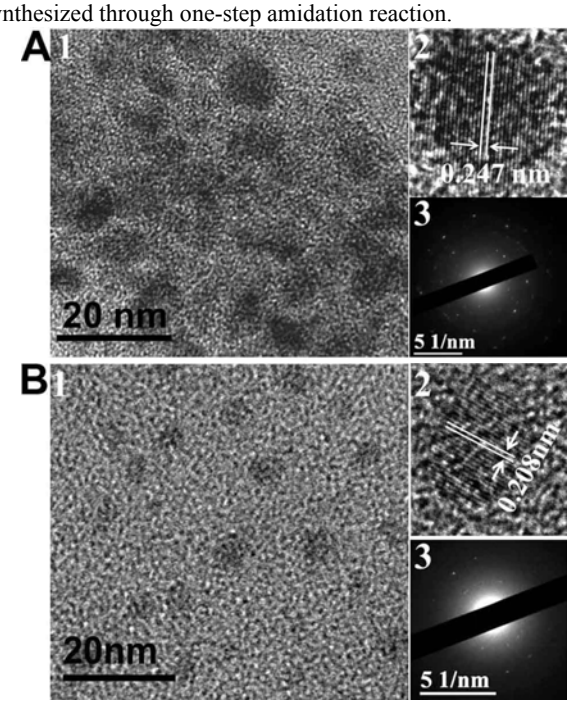

Fig.2 HR-TEM images of (A) ICG-FA-WCS NPs (a), lattice planes (b) and selected-area electron diffraction (SAED) pattern (c). HR-TEM images of (B) ICG-WCS NPs (a), lattice planes (b) and SAED pattern (c). NPs were self-assembled in pure water with the mass ratio of FA-WCS or WCS to ICG 25:1.

Fig. 2A (1) displays a typical HR-TEM image of the ICG-FA-WCS NPs of the mass ratio of FA-WCS to ICG=25:1 with an average diameter of ca. 10 nm. Interestingly, lattice planes with a space of 0.247 nm (Fig. 2A (2)) were identified in the nanostructures of ICG-FA-WCS NPs, which may be attributed to the (104) or (024) diffraction plane of chitosan observed in JCPDS cards 39-1894. Lattice planes with a space of 0.269 nm (Fig. S-2) are also observed, which is analogous to the (152) or (320) lattices of diffraction plane of chitosan (JCPDS 39-1894). The significant different crystalline nature of ICG-FA-WCS NPs may indicate that they are polycrystalline or contain significant quantities of other substance, like FA and ICG, which may be both involved in the formation of crystalline. The selected-area electron diffraction (SAED) pattern (Fig. 2A (3)) further confirms the characteristics of crystalline solid. Correspondingly, Fig. 2B(1) shows the HR-TEM image of the ICG-WCS NPs, the lattice planes (Fig. 2B (2)) and SAED pattern (Fig. 2B (3)), which reveals that the single core of ICG-WCS NPs is also crystalline. Only lattice planes with a space of 0.208 nm were observed in Fig. 2B (2). The crystallite structure characteristics of chitosan

was also reported in previous work which was produced by reprecipitation from formic acid.[30] The size distribution of ICG-FA-WCS NPs (Fig. S-3) is in the range of 4-15 nm, which is broader than that of ICG-WCS NPs (4-11 nm, Fig. S-4) due to the integration of FA moiety into the nanostructure of ICG-FA-WCS NPs.

The self-assembled NPs are crystalline might because that the FA-WCS with protonated amino groups in the hexosaminide backbone is positively charged under neutral conditions (pH=7.0) and the negatively charged ICG molecules are electrostatically attached along the FA-WCS chain. As a result, positively charged FA-WCS polymer strands adhered negatively charged ICG molecules can intertwine each other, resulting in the formation of compact three-dimensional nanostructure. Incorporating of the ICG into the WCS or FA-WCS causes a slight decrease of the zeta potential of the self-assembled NPs (Fig. S-5). This is the first report that crystal ICG-containing chitosan NPs can be prepared by a non-covalent self-assembly approach. Unlike the ordinary chitosan that is only soluble in an acidic solution, the WCS with a molecular weight of 19.8 KDa is highly water soluble at neutral pH, which is beneficial for its application as ICG carriers for intravenous (IV) injection of NPs in tumor optical imaging. Moreover, the synthesis takes only about 20 seconds which only involves water and inexpensive reagents. By rational selecting negatively charged drugs, genes and biomolecules as delivery cargoes, this strategy can be developed as a general method to fabricate multifunctional agents.

To further investigate the mass ratio of FA-WCS to ICG on the NPs' morphology, variation of the mass ratio of FA-WCS to ICG in a range of 10:1, 20:1, 25:1, 30:1 and 40:1 were chosen for the preparation of the self-assembled NPs. As shown in Fig. S-6, when the mass ratio of FA-WCS to ICG is 10:1, the prepared ICG-FA-WCS NPs were ~ 60 nm clusters of ultrasmall nanoparticles and the resulting NPs exhibited irregular shapes. This might due to the relatively large amount of ICG that limits the formation of regular ICG-FA-WCS NPs. The lattice planes with a space of 0.371 nm were observed in the HR-TEM image of ICG-FA-WCS NPs with the mass ratio of FA-WCS to ICG= 10:1(Fig. S-7). With the increase of the mass ratio of FA-WCS to ICG, the shapes of the self-assembled ICG-FA-WCS NPs became more and more spherical (Fig. S-6A, C, E, Fig. 2A) and the particle size distribution was narrowing dramatically (Fig. S-6B, D, F, Fig. S-3). As the mass ratio achieved 40:1, no NPs were observed with HE-TEM because there are no enough ICG molecules available for the self-assembling process. HR-TEM characterization proved that all the ICG-FA-WCS NPs were crystalline within the range of investigated mass ratio of FA-WCS to ICG. The lattice planes with spaces of 0.247 nm (Fig. S-8), 0.238 nm (Fig. S-9) were also observed for the ICG-FA-WCS NPs with the mass ratio of FA-WCS to ICG= 20:1 and 30:1, respectively. The data of particle size and size distribution were summarized in Table 1. The ultrasmall NPs with sizes <20 nm are believed to be more suitable for cellular and sub-cellular targeting in tumor molecular imaging because of their small sizes, large cellular uptake amount and long blood-circulation lifetime.[31] Since the HR-TEM image of ICG-FA-WCS NPs with the mass ratio of FA-WCS to ICG at 25:1 exhibits an average particle size about 10 nm. These NPs also have appropriate ICG-loading rate, therefore they were used in the following experiment for both *in vitro* and *in vivo* tumor imaging.

Table1: Various particle sizes and size distributions of the ICG-WSC or ICG-FA-WCS NPs with different mass ratio of FA-WCS or WCS to ICG self-assembled in ultrapure water

Mass ratio of FA-WCS or WCS to ICG	10:1	20:1	25:1	30:1	40:1
Size of ICG-FA-WCS NPs (nm)	63.4	12.3	10.0	4.7	NA
Size of ICG-WCS NPs (nm)	NA	NA	7.1	NA	NA
Size distribution of ICG-FA-WCS NPs (nm)	32-93	6.2-20	5.6-15.4	2.5-6.8	NA
Size distribution of ICG-WCS NPs (nm)	NA	NA	5.2-11.8	NA	NA

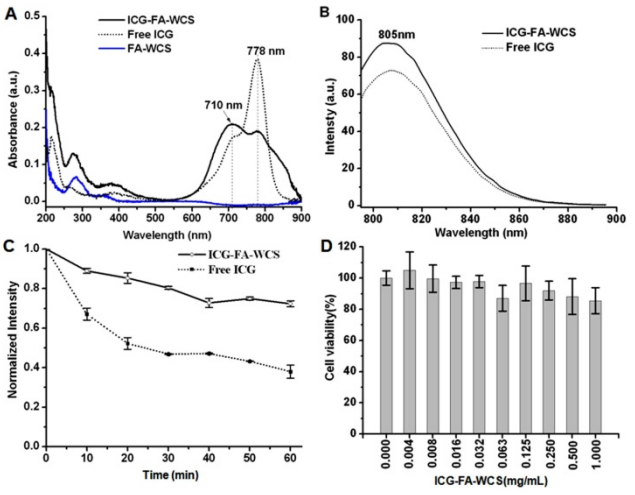

Fig. 3 Fluorescence images of various cells cultured with free ICG, ICG-WCS, ICG-FA-WCS NPs (mass ratio of WCS or FA-WCS to ICG = 25:1, 31μg·mL^{-1}, calculated for ICG). Quantitative fluorescence intensity of various cells cultured with free ICG, ICG-WCS, ICG-FA-WCS NPs (mass ratio of WCS or FA-WCS to ICG = 25:1, 31μg·mL^{-1}, calculated for ICG).

The optical properties of the ICG-FA-WCS were investigated. Fig. 3A shows the absorption and emission spectra of free ICG and ICG-FA-WCS in aqueous solution, respectively. In this condition, no detectable absorption and emission peaks were observed for the control FA-WCS, suggesting that the NIR fluorescence comes solely from ICG. After self-assembling, the absorption peak at 778 nm decreases, while the peak at 710 nm increases for ICG-FA-WCS NPs as compared to that of free ICG. This revealed that the ICG local environment was changed after forming the ICG-FA-WCS NPs, indicating the occurrence of self-assembling between ICG and FA-WCS. The emission peak at 805 nm for ICG-FA-WCS (Fig. 3B) did not shift after encapsulation of ICG with FA-WCS carrier. We then investigated the photostability of the prepared ICG-FA-WCS NPs by using the free ICG as control under the illumination with 60-W filament lamp as an excitation source. As shown in Fig. 3C, after 60 min illumination, the fluorescence intensity of ICG-FA-WCS NPs only decreases 28% compared to that of 62% for free ICG, demonstrating an improved photostability of ICG after self-assembling due to the FA-WCS shielding effect for ICG from optical degradation. As such, ICG-containing NPs with good

photostability are essential for their application in tumor molecular imaging. Moreover, ICG-FA-WCS NPs with low cytotoxicity and high photostability have shown tremendous promise as indicators for bioimaging.[15, 22, 32] To confirm their potential applications in optical imaging, the cytotoxicity of ICG-FA-WCS NPs was investigated by methyl thiazolyl tetrazolium (MTT) assay in CHO cells (Fig. 3D). After culturing for 24 h, the cell viability remains above 85% in the presence of a relatively high concentration of ICG-FA-WCS NPs (1.0 mg·mL^{-1}), displaying very low toxicity of the NPs to CHO cells. The lower cytotoxicity may be due to the use of biocompatible WCS and FA, which is essential for their further applications as fluorescent NPs for *in vivo* optical tumor imaging.

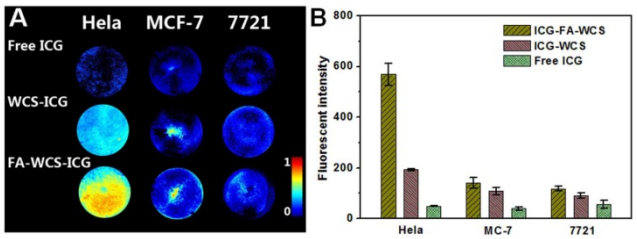

Fig. 4 Fluorescence images of various cells cultured with free ICG, ICG-WCS, ICG-FA-WCS NPs (mass ratio of WCS or FA-WCS to ICG = 25:1, 31μg·mL^{-1}, calculated for ICG). Quantitative fluorescence intensity of various cells cultured with free ICG, ICG-WCS, ICG-FA-WCS NPs (mass ratio of WCS or FA-WCS to ICG = 25:1, 31μg·mL^{-1}, calculated for ICG).

To demonstrate the applicability of ICG-FA-WCS NPs for selective targeting FR-expressing cells, an *in vitro* cell imaging study was carried out with FR-positive HeLa (human cervical cancer)[33], FR-negative cells (human breast cancer cells MCF-7 and human liver cancer cells 7721). As shown in Fig. 4A, there is no obvious difference of the fluorescence intensity for three cells incubated free ICG as determined with Maestro *in vivo* imaging system. Only HeLa cells treated with ICG-WCS NPs show greater fluorescence. Notably, HeLa cells exhibited much stronger fluorescence than MCF-7 and 7721 cells after these three kinds of cells were incubated with ICG-FA-WCS NPs. The fluorescence intensity of HeLa cells cultured with ICG-FA-WCS NPs was 3 and 3.9 times greater than that of MCF-7 and 7721 cells, respectively (Fig. 4B), clearly suggesting that ICG-FA-WCS NPs can serve as a fluorescence probe for imaging of FR-positive tumor cells.

We then evaluated the potential use of the ICG-FA-WCS NPs for *in vivo* tumor molecular optical imaging by utilizing free ICG and ICG-WCS as a non-targeted control in a HeLa xenograft model (2 μmol·kg^{-1} body weight, calculated for ICG) with the Maestro EX *in vivo* imaging system. Fig. 5 shows the representative whole-body NIR fluorescence images of nude mice administrated with free ICG, ICG-WCS and ICG-FA-WCS NPs at 10 min, 1, 48, 72 and 96 h time points, respectively. Strong NIR fluorescence signal was observed in the belly during the first 1 h post-injection and it is difficult to get clear tumor image because of the NPs circulation in the bloodstream (Fig. 5 (a1-a2), (b1-b2) and (c1-c2)). Likewise, Cai and co-workers also found the fluorescence signal was located in the belly at 0.5 h after injection of ICG-doped PLGA lipid nanoparticles (FA-ICG-PLGA-lipid NPs) in human breast tumor-bearing mice.[34] At 48 h, it appears that the majority of the background NIR fluorescence signal was cleared and the tumor with ICG-FA-WCS NPs (Fig. 5(c3)) exhibited greater and prolonged fluorescence signal as compared to those of the free ICG (Fig. 5(a3)) and non-targeted ICG-WCS NPs (Fig. 5(b3)). The ICG-FA-WCS NPs resulted in strong prolonged enhancement in tumor tissue for at least 96 h post-injection, indicating effective binding of the targeted agent in the tumor tissue. The prolonged persistence of the FA targeted NPs in animal is remarkable and consistent with most polymeric deliver systems.[35-37] The extended circulation of the NPs is useful for the effective delivery of the agent to the interest site and decreasing the accumulation of the agents in the major organ, such as liver. Quantitative analysis of fluorescence signal (Fig. 5B) revealed that the ICG-FA-WCS NPs resulted in approximately 117% and 158% increase in fluorescence signal as compared to free ICG at 48 h and 72 h, respectively. As a contrast, the ICG-WCS only resulted in 48% and 50% signal increase in the tumor region. Not only we observed the passive targeting effect of ICG-WCS NPs, but also the interesting active targeting effect from ICG-FA-WCS NPs due to the introduction of FA conjugated onto the WCS matrix for ICG delivery. These results demonstrate that ICG-FA-WCS NPs were able to substantially and preferentially localize in tumor tissue *in vivo*.

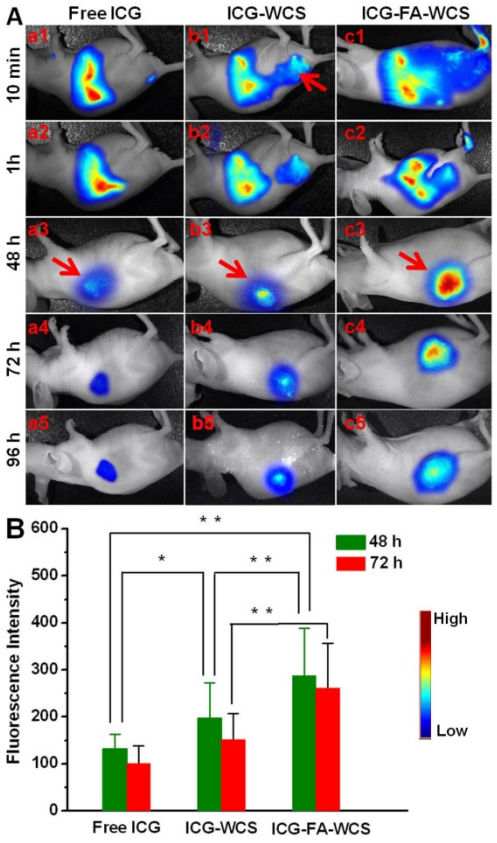

Fig.5 (A) *In vivo* fluorescence imaging of human cervical tumor-bearing nude mice intravenously injected with free ICG (a1-a5), ICG-WCS (b1-b5) and ICG-FA-WCS (c1-c5) NPs (mass ratio of WCS or FA-WCS to ICG = 25:1, 2 μmol·kg^{-1} body weight, calculated for ICG) with the Maestro EX *in vivo* imaging system. (*N*=6). Arrows indicate tumors. (B) Relative fluorescence intensity in tumors of nude mice after injected with free ICG, ICG-WCS and ICG-FA-WCS NPs at 48 h and 72 h, respectively. (*P < 0.05, **P < 0.01).

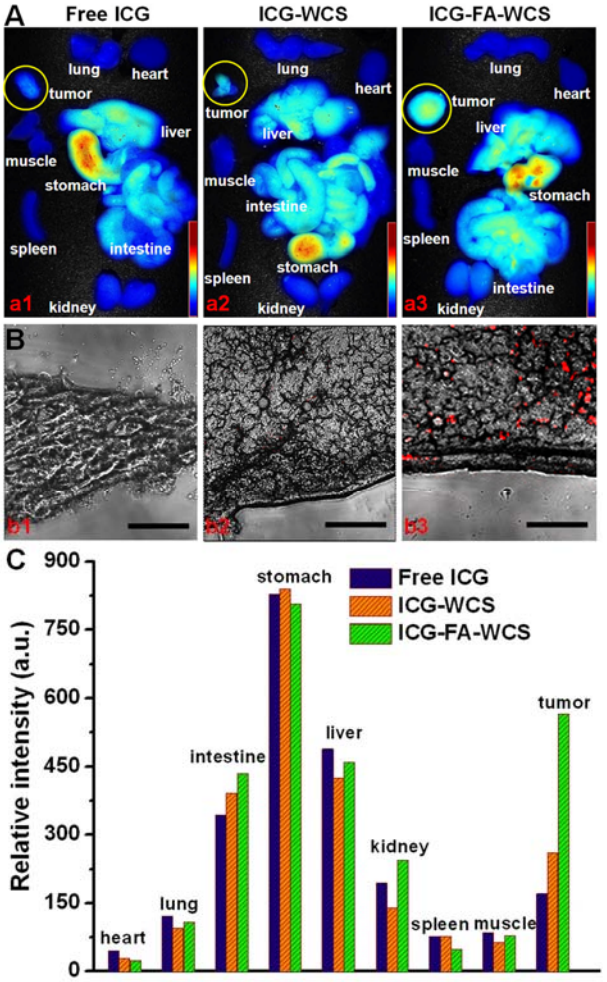

Fig. 6 Representative fluorescence images of the tumor and major organs/tissues for the nude mice intravenously injected with free ICG (a1), ICG-WCS (a2) and ICG-FA-WCS NPs (a3) at 48 h (A). Yellow circle shows the tumor. Histological analysis of tumor tissue injected with free ICG (b1), ICG-WCS (b2) and ICG-FA-WCS NPs (b3) at 48 h (B) (Scale bar = 300 μm).

The binding specificity of ICG-FA-WCS NPs to the human cervical tumor was further investigated by *ex vivo* fluorescence imaging of the tumor and major organs/tissues at 48 h post-injection. As shown in Fig. 6A, strong fluorescence was observed in the cervical tumor from the mouse injected with ICG-FA-WCS NPs, whereas little fluorescence was detected in the tumor with free ICG and ICG-WCS NPs. Moreover, intense fluorescence was observed in the stomach, liver and intestine because ICG would be released after catabolism of the assembled nanostructure and would then gradually accumulate into the liver, and finally be excreted via the hepatobiliary system.[8, 16] Notably, the histological analysis of tumor tissue injected with free ICG, ICG-WCS and ICG-FA-WCS NPs at 48 h demonstrated that significant fluorescence signal was found in the tumor slice with ICG-FA-WCS NPs (Fig. 6B(b3)). Therefore, these NPs were able to specifically bind to the tumor tissue and resulted in enhanced fluorescence in tumor imaging. More quantitatively, fluorescence signal of the tumor and major organs/tissues at 48 h post-injection was shown in Fig. 6C. Fluorescence intensity in tumors of the mice injected with ICG-FA-WCS NPs was 3.3 and 2.2 times greater than that of the mice injected with free ICG and ICG-WCS, respectively. Thus, the tumor selectivity was improved by active targeting via FA-FRs interactions, which are well consistent with the result of *in vivo* imaging (Fig. 5).

4. Conclusions

In conclusion, we have successfully constructed crystalline ultrasmall ICG-containing NPs from a facile self-assembled method for *in vivo* tumor targeted molecular imaging. The as-prepared NIR FA-WCS-ICG NPs exhibited good photostability, lower cytotoxicity due to the use of biocompatible and nontoxic FA modified water-soluble chitosan as nano-carriers. Significant tumor accumulation was observed for both *in vivo* and *in vitro* tumor imaging, verifying that the self-assembled crystal ICG-containing nanoparticles have the potential for simultaneous tumor targeting and NIR tumor molecular imaging. It is anticipated that the self-assembled crystal nanostructures as prepared by such convenient approach from chitosan may provide a variety of nano-methodologies for fabricating other multifunctional agents for further tumor theranosis applications and studies.

Author Contributions

‖Hao Wu and Haidong Zhao contributed equally to this work.

Acknowledgements

This work was supported by the National Nature Science Foundation of China (91227126), National Special Fund for Key Scientific Instrument and Equipment Development (2013YQ17046307) and the Nature Science Foundation of Liaoning Province, China (2013020177). We are grateful to Ms Xiaoxi Xu, Guoshuang Zheng and Mr. Yan Lv for experimental help.

Notes and references

[a]*Division of Biotechnology, Dalian Institute of Chemical Physics, Chinese Academy of Sciences, 457 Zhongshan Road, Dalian 116023, China; Fax: +86-411-84379139; maxj@dicp.ac.cn; mqtan@dicp.ac.cn*
[b] *University of the Chinese Academy of Sciences, Beijing 100049, China;*
[c] *The Second Affiliated Hospital of Dalian Medical University, 467 Zhongshan Road, Dalian 116023, China*

† Electronic Supplementary Information (ESI) available: [details of ^{1}H NMR spectra of FA-WCS and WCS, additional HRTEM images, Zeta potential of NPs, and details of Figs. S1 to S9]. See DOI: 10.1039/b000000x/

1. J. Choi, J. Yang, J. Park, E. Kim, J. S. Suh, Y. M. Huh and S. Haam, Adv Funct Mater, 2011, 21, 1082-1088.
2. K. Chen, L. P. Yap, R. Park, X. L. Hui, K. C. Wu, D. M. Fan, X. Y. Chen and P. S. Conti, Amino Acids, 2012, 42, 1329-1337.
3. F. K. Swirski, C. R. Berger, J. L. Figueiredo, T. R. Mempel, U. H. von Andrian, M. J. Pittet and R. Weissleder, Plos One, 2007, 2, e1075.
4. P. P. Ghoroghchian, P. R. Frail, K. Susumu, D. Blessington, A. K. Brannan, F. S. Bates, B. Chance, D. A. Hammer and M. J. Therien, P Natl Acad Sci USA, 2005, 102, 2922-2927.
5. S. L. Luo, E. L. Zhang, Y. P. Su, T. M. Cheng and C. M. Shi, Biomaterials, 2011, 32, 7127-7138.
6. J. Li, S. P. Song, X. F. Liu, L. H. Wang, D. Pan, Q. Huang, Y. Zhao and C. H. Fan, Adv Mater, 2008, 20, 497-500.
7. S. Kim, H. E. Pudavar, A. Bonoiu and P. N. Prasad, Adv Mater, 2007, 19, 3791-3795.
8. P. Ott, Pharmacol Toxicol, 1998, 83, 7-48.

9. S. Afonso, I. Miranda, R. Matos, R. Moreno, P. Amado and F. O. Martins, Intens Care Med, 2009, 35, 130-130.
10. J. H. Francis, D. H. Abramson, S. E. Brodie and B. P. Marr, Brit J Ophthalmol, 2013, 97, 164-168.
11. J. M. I. Maarek, D. P. Holschneider, J. Harimoto, J. Yang, O. U. Scremin and E. H. Rubinstein, Anesthesiology, 2004, 100, 1476-1483.
12. B. E. Schaafsma, J. S. D. Mieog, M. Hutteman, J. R. Van der Vorst, P. J. K. Kuppen, C. Lowik, J. V. Frangioni, C. J. H. Van de Velde and A. L. Vahrmeijer, J Surg Oncol, 2011, 104, 323-332.
13. J. Yu, D. Javier, M. A. Yaseen, N. Nitin, R. Richards-Kortum, B. Anvari and M. S. Wong, J Am Chem Soc, 2010, 132, 1929-1938.
14. G. R. Cherrick, S. W. Stein, C. M. Leevy and C. S. Davidson, J Clin Invest, 1960, 39, 592-600.
15. T. H. Kim, Y. P. Chen, C. W. Mount, W. R. Gombotz, X. D. Li and S. H. Pun, Pharmaceut Res, 2010, 27, 1900-1913.
16. A. K. Kirchherr, A. Briel and K. Mader, Mol Pharmaceut, 2009, 6, 480-491.
17. V. Saxena, M. Sadoqi and J. Shao, J Photoch Photobio B, 2004, 74, 29-38.
18. V. Saxena, M. Sadoqi and J. Shao, Int J Pharm, 2004, 278, 293-301.
19. H. Y. Zhu, F. Liu, J. Guo, J. P. Xue, Z. Y. Qian and Y. Q. Gu, Carbohyd Polym, 2011, 86, 1118-1129.
20. E. I. Altinoglu, T. J. Russin, J. M. Kaiser, B. M. Barth, P. C. Eklund, M. Kester and J. H. Adair, Acs Nano, 2008, 2, 2075-2084.
21. C. H. Lee, S. H. Cheng, Y. J. Wang, Y. C. Chen, N. T. Chen, J. Souris, C. T. Chen, C. Y. Mou, C. S. Yang and L. W. Lo, Adv Funct Mater, 2009, 19, 215-222.
22. X. H. Zheng, D. Xing, F. F. Zhou, B. Y. Wu and W. R. Chen, Mol Pharmaceut, 2011, 8, 447-456.
23. I. Y. Kim, S. J. Seo, H. S. Moon, M. K. Yoo, I. Y. Park, B. C. Kim and C. S. Cho, Biotechnol Adv, 2008, 26, 1-21.
24. J. L. Zhang, W. S. Xia, P. Liu, Q. Y. Cheng, T. Tahirou, W. X. Gu and B. Li, Mar Drugs, 2010, 8, 1962-1987.
25. J. Gong, X. L. Hu, K. W. Wong, Z. Zheng, L. Yang, W. M. Lau and R. X. Du, Adv Mater, 2008, 20, 2111-2115.
26. T. L. Kalber, N. Kamaly, P. W. So, J. A. Pugh, J. Bunch, C. W. McLeod, M. R. Jorgensen, A. D. Miller and J. D. Bell, Mol Imaging Biol, 2011, 13, 653-662.
27. D. Pan, J. L. Turner and K. L. Wooley, Chem Commun, 2003, 2400.
28. W. Xia and P. S. Low, J Med Chem, 2010, 53, 6811-6824.
29. N. Kubota, N. Tatsumoto, T. Sano and K. Toya, Carbohyd Res, 2000, 324, 268-274.
30. E. L. Mogilevskaya, T. A. Akopova, A. N. Zelenetskii and A. N. Ozerin, Polymer Science, Ser. A, 2006, 48, 116-123.
31. V. P. Torchilin, Adv Drug Deliver Rev, 2012, 64, 302-315.
32. X. H. Zheng, F. F. Zhou, B. Y. Wu, W. R. Chen and D. Xing, Mol Pharmaceut, 2012, 9, 514-522.
33. D. Feng, Y. C. Song, W. Shi, X. H. Li and H. M. Ma, Anal Chem, 2013, 85, 6530-6535.

Self-assembly-induced near-infrared fluorescence nanoprobes exhibiting spontaneous lattices were prepared and evaluated for *in vitro* and *in vivo* tumor molecular imaging.